Single-Shot Readout of Multiple Nuclear Spin Qubits in Diamond under Ambient Conditions

A. Dréau,[1] P. Spinicelli,[1] J. R. Maze,[2] J.-F. Roch,[3] and V. Jacques[1,3,*]

[1]*Laboratoire de Photonique Quantique et Moléculaire, Ecole Normale Supérieure de Cachan and CNRS UMR 8537, 94235 Cachan, France*

[2]*Facultad de Física, Pontificia Universidad Católica de Chile, Santiago 7820436, Chile*

[3]*Laboratoire Aimé Cotton, CNRS UPR 3321 and Université Paris-Sud, 91405 Orsay, France*

(Received 23 October 2012; published 5 February 2013)

We use the electronic spin of a single nitrogen-vacancy defect in diamond to observe the real-time evolution of neighboring single nuclear spins under ambient conditions. Using a diamond sample with a natural abundance of ^{13}C isotopes, we first demonstrate high fidelity initialization and single-shot readout of an individual ^{13}C nuclear spin. By including the intrinsic ^{14}N nuclear spin of the nitrogen-vacancy defect in the quantum register, we then report the simultaneous observation of quantum jumps linked to both nuclear spin species, providing an efficient initialization of the two qubits. These results open up new avenues for diamond-based quantum information processing including active feedback in quantum error correction protocols and tests of quantum correlations with solid-state single spins at room temperature.

DOI: 10.1103/PhysRevLett.110.060502 PACS numbers: 03.67.Lx, 42.50.Ct, 42.50.Lc, 76.30.Mi

Nuclear spins are attractive candidates for solid-state quantum information storage and processing owing to their extremely long coherence time [1–3]. However, since this appealing property results from a high level of isolation from the environment, it remains a challenging task to polarize, manipulate, and readout with high fidelity individual nuclear spins [4]. A promising approach to overcome this limitation consists of utilizing an ancillary single electronic spin to detect and control remote nuclear spins coupled by hyperfine interaction [5–10]. In this context, the nitrogen-vacancy (NV) defect in diamond has recently attracted considerable interest because its electronic spin can be polarized, coherently manipulated, and readout by optical means with long coherence times, even under ambient conditions [11]. The NV's electronic spin thus behaves as an ultrasensitive magnetometer at the nanoscale [12], providing a robust interface to detect and control nearby nuclear spins in the diamond lattice. This approach has been used in the past years to study the coherent dynamics of multispin systems [13], to perform universal quantum gates [14,15] and to develop few-qubits quantum registers, where single nuclear spins are used as quantum memories [7,16,17]. A second-long coherence time was recently demonstrated for a single ^{13}C nuclear spin weakly coupled to a single NV defect in an isotopically purified diamond sample [10]. This result, combined with the ability to perform spin-photon entanglement [18] and two-photon interference from distant NV defects at low temperature [19,20], makes single spins in diamond a promising building block for quantum repeaters and long-distance quantum communications.

However, advanced quantum algorithms such as quantum error correction protocols require high fidelity initialization and single-shot readout over multiple qubits [21]. Along the line of recent works directed towards this goal [8–10,22], we first report high fidelity single-shot readout of an individual ^{13}C nuclear spin by using the electronic spin of a single NV defect as an ancillary qubit in a diamond sample with a natural abundance of ^{13}C isotopes (1.1%). Repetitive readout indicates a polarization lifetime exceeding seconds at moderate magnetic fields, which illustrates the robustness of the ^{13}C nuclear spin state. Then, we demonstrate efficient initialization of two nuclear spin qubits in a well-defined state by adding the ^{14}N nucleus of the NV defect in the quantum register.

The spin system considered in this study is depicted in Figs. 1(a) and 1(b). The electronic spin ($S = 1$) of a single NV defect is coupled by hyperfine interaction with both its intrinsic ^{14}N nuclear spin ($I = 1$) and a neighboring ^{13}C nuclear spin ($I = 1/2$). A permanent magnet placed on a three-axis translation stage is used to apply a static magnetic field along the NV defect axis and the spin transition between the $m_s = 0$ and $m_s = -1$ electron spin manifolds is coherently driven through microwave (MW) excitation [23]. As shown in Fig. 1(c), the hyperfine structure of the spin system, recorded through pulsed-ESR spectroscopy [24], exhibits six nuclear-spin conserving transitions. From this spectrum, recorded for a magnetic field magnitude $B = 2000$ G, we extract the projected strength of the ^{13}C hyperfine interaction $\mathcal{A}_{\parallel} = \mathcal{A}_{zz} = 258 \pm 10$ kHz [23]. We obtain further qualitative information of the hyperfine interaction through dynamic polarization measurements at the excited-state level anticrossing (ESLAC) [25]. The ^{13}C polarization efficiency was estimated by using the Fourier transform of the free-induction decay (FID) signal measured by applying a Ramsey sequence $\frac{\pi}{2} - \tau - \frac{\pi}{2}$ to the NV defect electron spin. Figure 1(d) shows the FID signal recorded at the ESLAC. Since the ^{14}N nuclear spin is perfectly polarized, the characteristic beating is linked to the weakly coupled ^{13}C nuclear spin. The Fourier

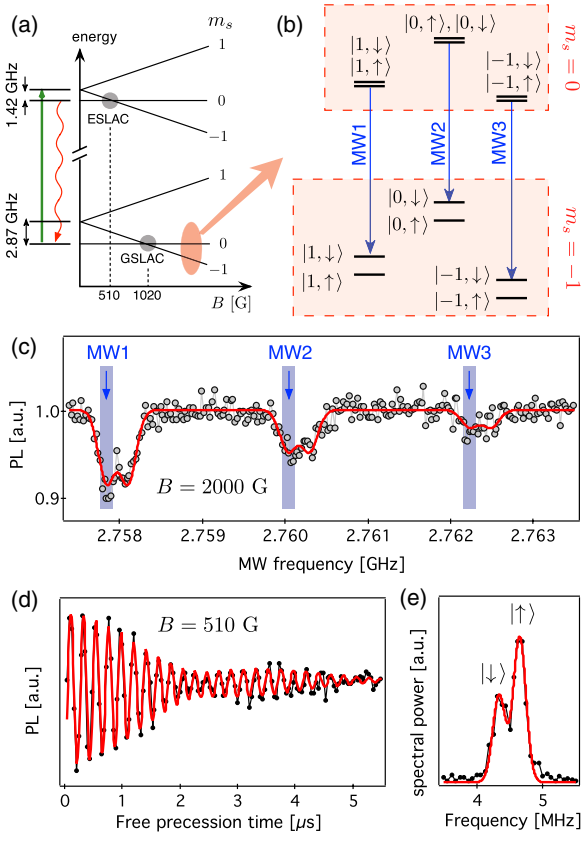

FIG. 1 (color online). (a) Energy-level diagram of the NV defect as a function of the strength of a static magnetic field B applied along the NV defect axis. Level anticrossings in the ground state (GSLAC) and in the excited state (ESLAC) are highlighted. (b) Hyperfine structure of the $m_s = 0$ and $m_s = -1$ electron spin manifolds for a NV defect coupled with its intrinsic ^{14}N nuclear spin ($m_{I^{(N)}}$) and with a nearby single ^{13}C nuclear spin ($\uparrow$ or $\downarrow$). The hyperfine sublevels are denoted as $|m_{I^{(N)}}, \uparrow(\downarrow)\rangle$. Blue arrows indicate the microwave (MW) transitions used for single-shot readout measurements. (c) Optically detected ESR spectrum recorded for a magnetic field $B \approx 2000$ G. (d) FID signal of the NV defect electron spin recorded at the ESLAC ($B \approx 510$ G) showing a coherence time $T_2^* = 2.9 \pm 0.1$ μs. (e) Fourier transform of the FID signal.

transform of the FID signal indicates a relatively high polarization efficiency $\mathcal{P} = 40 \pm 10\%$, which suggests that the ^{13}C quantization axis is close to the NV defect axis in both the ground and excited states [26]. The anisotropic component of the hyperfine tensor $\mathcal{A}_{\text{ani}}$ is therefore assumed to be much smaller than $\mathcal{A}_{zz}$. Since the ^{13}C nuclear spin gets polarized in $|\uparrow\rangle$, this measurement also provides unambiguous identification of each ESR frequency to a given nuclear spin state, $|\uparrow\rangle$ or $|\downarrow\rangle$ [27,28].

In the spirit of previous works [9,10], projective single-shot detection of the ^{13}C nuclear spin state is achieved by accumulating the NV defect photoluminescence (PL) while repeating the sequence depicted in Fig. 2(a). The NV defect electron spin is first initialized into the $m_s = 0$ sublevel through optical pumping. A controlled not (CNOT) gate is then applied to induce an electron spin flip conditioned on the ^{13}C nuclear spin state $|\psi_n\rangle$. Finally, the resulting electronic spin state is optically readout by applying a 300-ns laser pulse. This sequence is repeated many times in order to increase the signal to noise ratio. The CNOT gate is experimentally realized by applying narrow-band MW π pulses on the electronic spin, which selectively drive the ESR transition for a given ^{13}C nuclear spin state, e.g., $|\downarrow\rangle$. In order to take advantage of the full ESR contrast and to get rid off any quantum jumps linked to the ^{14}N nuclear spin [9], three MW sources are used for driving simultaneously ^{13}C nuclear spin state-selective transitions from each hyperfine sublevels linked to the ^{14}N nucleus [Figs. 1(b) and 1(c)].

A typical PL time trace recorded while continuously repeating the sequence is shown in Fig. 2(b). For each data point, the PL signal is accumulated during $\tau_b = 120$ ms, corresponding to approximatively 20000 repetitions of the readout sequence. The signal exhibits well-defined quantum jumps linked to the evolution of the ^{13}C nuclear spin state. Indeed, when the nuclear spin is in state $|\downarrow\rangle$, the CNOT gate flips the NV defect electron spin, $m_s = 0 \rightarrow m_s = -1$, and a low PL signal is observed (*dark* state) owing to spin-dependent PL of the NV defect. Conversely, when the nuclear spin is in state $|\uparrow\rangle$, the electron spin remains in the $m_s = 0$ sublevel at each repetition of the sequence and a high PL signal is observed (*bright* state). Nuclear spin flips are therefore evidenced in real time as abrupt jumps between two distinct values of the PL signal. For a magnetic field $B = 1610$ G applied along the NV defect axis, we infer the characteristic relaxation times of the ^{13}C nuclear spin while applying repetitive readout $T_{1,\uparrow(\text{bright})} = 2.4 \pm 0.1$ s and $T_{1,\downarrow(\text{dark})} = 1.5 \pm 0.2$ s.

To estimate the readout fidelity, the ^{13}C nuclear spin is first deterministically initialized in a given state through a single-shot readout measurement. By introducing an initialization threshold $\mathcal{N}_{i,\downarrow}$ ($\mathcal{N}_{i,\uparrow}$), photon counting events such that $\mathcal{N} < \mathcal{N}_{i,\downarrow}$ ($\mathcal{N} > \mathcal{N}_{i,\uparrow}$) are postselected, corresponding to an initialization in state $|\downarrow\rangle$ ($|\uparrow\rangle$). Using $\mathcal{N}_{i,\downarrow} = 615$ counts and $\mathcal{N}_{i,\uparrow} = 845$ counts, the initialization fidelity exceeds 99% for both nuclear spin states [see Fig. 2(d)]. After successful initialization, a subsequent readout measurement is performed allowing us to build the nuclear-spin dependent photon counting distributions $\mathcal{S}_{\uparrow(\downarrow)}$ [23]. As shown in Fig. 2(c), the distributions linked to each nuclear spin state can be clearly distinguished and the readout fidelities $\mathcal{F}_{\uparrow(\downarrow)}$ are defined as

$$\mathcal{F}_{\downarrow(\uparrow)}(\mathcal{N}_r) = \frac{\int_{0(\mathcal{N}_r)}^{\mathcal{N}_r(\infty)} \mathcal{S}_{\downarrow(\uparrow)}(\mathcal{N}) d\mathcal{N}}{\int_{0(\mathcal{N}_r)}^{\mathcal{N}_r(\infty)} [\mathcal{S}_{\downarrow} + \mathcal{S}_{\uparrow}](\mathcal{N}) d\mathcal{N}}, \qquad (1)$$

where $\mathcal{N}_r$ is the readout threshold. For $\mathcal{N}_{r,\text{opt}} = 735$ counts, corresponding to the maximum overlap between the two photon-counting distributions, we extract

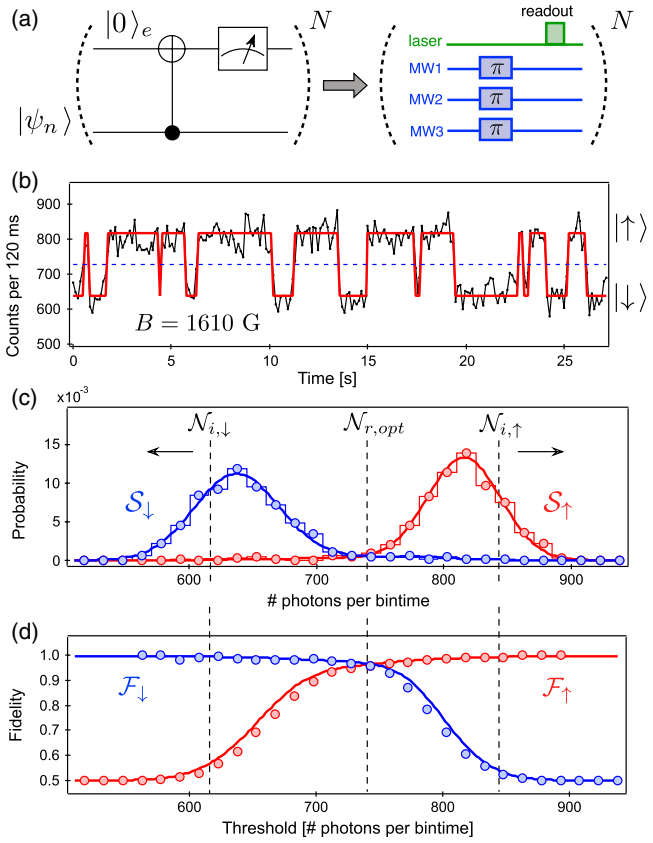

FIG. 2 (color online). (a) Logic diagram of the single-shot readout scheme and corresponding experimental sequence. The duration of the π-pulses is set to 4 μs. The 300-ns laser pulse is used both for spin-state read-out and to achieve an efficient preparation of the NV defect electron spin in the $m_s = 0$ sublevel ($|0\rangle_e$) at each repetition of the sequence. (b) PL time trace showing quantum jumps of the ^{13}C nuclear spin state. The solid line is a fit with a two states hidden Markov model from which the relaxation time T_1 of the nuclear spin state is extracted. (c) Normalized nuclear-spin dependent photon counting distributions $\mathcal{S}_{\uparrow(\downarrow)}$. The solid lines are data fitting with the formula given in Ref. [23]. (d) Single-shot readout fidelity $\mathcal{F}_{\uparrow(\downarrow)}$ as a function of the readout threshold. The initialization thresholds $\mathcal{N}_{i,\downarrow}$,$\mathcal{N}_{i,\uparrow}$ and the optimized discrimination threshold $\mathcal{N}_{r,\mathrm{opt}}$ are indicated with dashed lines. The solid lines are extracted from the fits in (c). We note that the initialization fidelity in state $|\downarrow\rangle$ ($|\uparrow\rangle$) is given by $\mathcal{F}_\downarrow(\mathcal{N}_{i,\downarrow})$ [$\mathcal{F}_\uparrow(\mathcal{N}_{i,\uparrow})$].

$\mathcal{F}_\downarrow = \mathcal{F}_\uparrow = 96 \pm 1.2\%$ [Fig. 2(d)]. This fidelity could be significantly improved by increasing the collection efficiency with diamond photonic nanostructures [29]. In addition, the selective MW π pulses used for the CNOT gate have a duration of 4 μs, corresponding to a spectral width of 130 kHz. Given the inhomogeneous linewidth of the ESR signal combined with the hyperfine coupling strength, the π pulses are therefore not perfectly selective leading to a decreased contrast of the projective measurement, which degrades the readout fidelity. This limitation could be overcome by using a CVD-grown diamond sample isotopically enriched with ^{12}C atoms, in which the inhomogeneous dephasing rate of the NV defect electron spin can reach a few kHz [10,11].

We now study the processes leading to nuclear spin depolarization. For a magnetic field B applied along the NV defect axis (z), the ground-state spin Hamiltonian reads $\mathcal{H} = \mathcal{H}_0 + \gamma_n B\hat{I}_z + \hat{\mathbf{S}}\cdot\mathcal{A}\cdot\hat{\mathbf{I}}$, where $\mathcal{H}_0$ includes both the pure electronic spin terms and the hyperfine interaction with the intrinsic ^{14}N nuclear spin, γ_n is the ^{13}C gyromagnetic ratio and $\mathcal{A}$ its hyperfine tensor. In the secular approximation, this Hamiltonian simplifies to

$$\mathcal{H} = \mathcal{H}_0 + \gamma_n B\hat{I}_z + \mathcal{A}_{zz}\hat{S}_z\hat{I}_z + \frac{\mathcal{A}_{\mathrm{ani}}}{2}[e^{-i\phi}\hat{S}_z\hat{I}_+ + e^{+i\phi}\hat{S}_z\hat{I}_-], \quad (2)$$

where $\mathcal{A}_{\mathrm{ani}} = (\mathcal{A}_{zx}^2 + \mathcal{A}_{zy}^2)^{1/2}$, $\tan\phi = \mathcal{A}_{zy}/\mathcal{A}_{zx}$ and $\hat{I}_\pm = \hat{I}_x \pm i\hat{I}_y$. The anisotropic component $\mathcal{A}_{\mathrm{ani}}$ of the hyperfine tensor therefore induces nuclear spin flips, leading to depolarization at a rate [23]

$$\gamma_1 = \frac{1}{T_1} \propto \frac{\mathcal{A}_{\mathrm{ani}}^2}{\mathcal{A}_{\mathrm{ani}}^2 + (\mathcal{A}_{zz} - \gamma_n B)^2}. \quad (3)$$

Considering this process as the main source of depolarization, the nuclear spin relaxation time might exhibit a quadratic dependence with the applied magnetic field. The experimental results depicted in Fig. 3 confirm this behavior at high fields, while two drops can be observed around $B \sim 510$ G and $B \sim 1020$ G, corresponding to level anti-crossings in the excited state and in the ground state, respectively [30] [Fig. 1(a)]. Around such magnetic field strengths, the secular approximation is not valid and additional electron-nuclear spin flip-flop terms $\mathcal{A}_\perp[\hat{S}_-\hat{I}_+ + \hat{S}_+\hat{I}_-]/2$ need to be added to the Hamiltonian [25,26], where $\mathcal{A}_\perp = (\mathcal{A}_{xx} + \mathcal{A}_{yy})/2$. As shown in Fig. 3, the experimental data are well fitted by a simple model including

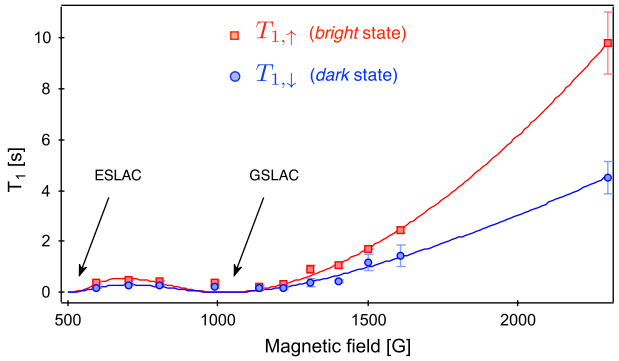

FIG. 3 (color online). Nuclear spin relaxation time T_1 as a function of the magnetic field strength for the *bright* state (red) and the *dark* state (blue). The solid lines are data fitting with a simple model including nuclear spin flips induced by the transverse component of the hyperfine tensor and electron-nuclear spin flip flops at the GSLAC and ESLAC [23].

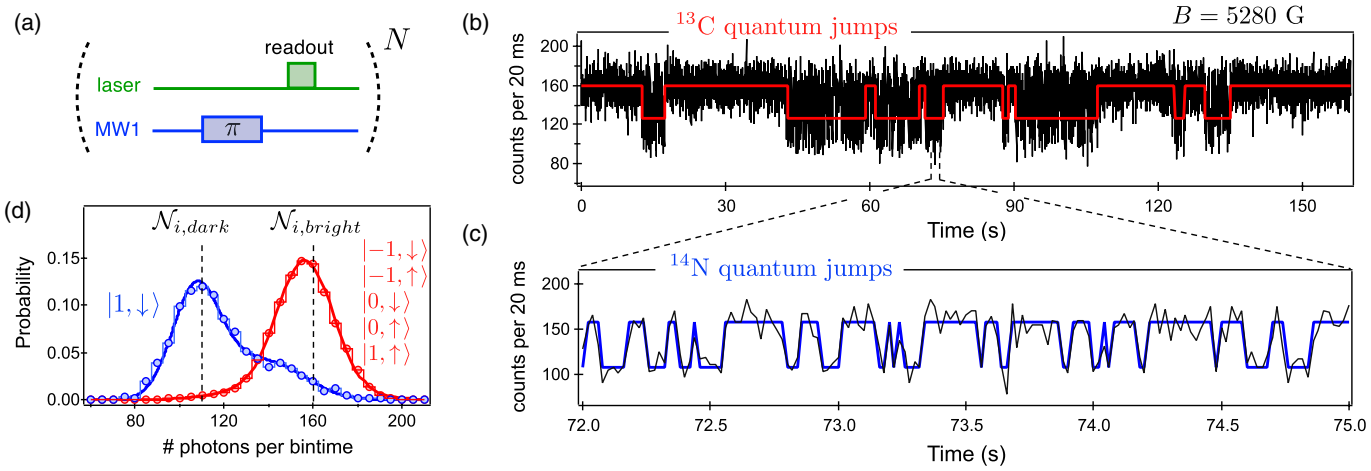

FIG. 4 (color online). (a) Experimental sequence. (b), (c) PL time trace recorded by continuously repeating the sequence for a magnetic field $B = 5280$ G. Each data point corresponds to approximatively 3000 repetitions of the readout sequence (20 ms). Quantum jumps linked to (b) the weakly coupled ^{13}C nuclear spin and to (c) the intrinsic ^{14}N nuclear spin can be distinguished. (d) Normalized nuclear-spin dependent photon counting distributions measured with the initialization thresholds set to $\mathcal{N}_{i,\mathrm{dark}} = 110$ counts and $\mathcal{N}_{i,\mathrm{bright}} = 160$ counts. The projective readout fidelity is optimized for a discrimination threshold $\mathcal{N}_{r,\mathrm{opt}} = 135$ counts.

depolarization induced by the anisotropic hyperfine interaction and spin mixing at the level anticrossings [23]. We note that the *bright* state always exhibits a longer relaxation time than the *dark* state. Furthermore, this effect is independent on the nuclear spin state used as the control state in the CNOT gate and is intrinsically linked to the readout process. Indeed, when the *dark* state is detected, a shorter nuclear spin lifetime is always observed because in this case the system spends on average more time in the $m_s = -1$ electronic spin sublevel, for which the anisotropic component of the hyperfine tensor induces nuclear spin flips [31].

According to Eq. (3), a long nuclear spin lifetime can be observed either for a ^{13}C nuclear spin with a weak anisotropic component of the hyperfine interaction, i.e., placed on a lattice site with a small angle with respect to the NV defect axis, or for an applied magnetic field such that $\gamma_n B \gg (\mathcal{A}_{zz}, \mathcal{A}_{\mathrm{ani}})$. In a diamond sample with a natural abundance of ^{13}C isotope (1.1%), the ESR linewidth is on the order of 200 kHz, which puts a limit to the weakest detectable hyperfine coupling strength in conventional ESR spectroscopy [Fig. 1(c)]. Apart from the ^{13}C nuclear spin studied in detail in this work, quantum jumps were also observed for a ^{13}C coupling strength $\mathcal{A}_{zz} = 380 \pm 10$ kHz (lattice site O in Ref. [28]) with a much shorter relaxation time [23]. For stronger hyperfine coupling strengths, the nuclear spin lifetime was not long enough to observe quantum jumps in the PL time trace for magnetic fields up to 5000 G. The probability to find weakly coupled ^{13}C nuclear spins would be significantly improved by using isotopically purified diamond samples [10]. However, we note that the speed of the single-shot readout measurement decreases with the ^{13}C coupling strength owing to the required spectral selectivity of the quantum logic.

Finally, we demonstrate single-shot readout in a two-qubit register by including the intrinsic ^{14}N nuclear spin of the NV defect. For this experiment, the CNOT gate is performed with a single narrow band MW π pulse which selectively drives the ESR transition for a given state of the register, e.g., state $|1,\downarrow\rangle$ [Fig. 1(b) and 1(a)]. The PL time trace then exhibits quantum jumps linked to both nuclear spin species, which can be easily distinguished because their characteristic relaxation times differ by orders of magnitude [Figs. 4(b) and 1(c)]. Indeed, although the ^{14}N nuclear spin shares its symmetry axis with the NV defect ($\mathcal{A}_{\mathrm{ani}} = 0$), its relaxation time is only a few tens of milliseconds because a strong hyperfine contact interaction in the NV defect excited state $\mathcal{A}_{\perp} \approx 40$ MHz induces fast electron-nuclear spin flip flops [9]. From the nuclear-spin dependent photon counting distributions, we infer that the two nuclear spin qubits can be initialized into state $|1,\downarrow\rangle$ (*dark* state) with a fidelity higher than 98% by using an initialization threshold $\mathcal{N}_{i,\mathrm{dark}} = 110$ counts [Figs. 4(d)]. We note that any state of the register could be deterministically prepared and readout by changing the frequency of the MW used for the CNOT gate. From the overlap between the photon counting distributions, we extract a projective readout fidelity $\mathcal{F} = 83 \pm 2\%$, limited by the ^{14}N nuclear spin relaxation time. This value could be significantly improved by increasing the magnetic field strength in order to decouple more efficiently the ^{14}N nuclear spin from the electron spin dynamics [9].

The reported initialization and single-shot readout of two nuclear spin qubits combined with well-established techniques of coherent manipulation within the quantum register [14,15] pave the way towards tests of quantum correlations with solid-state single spins at room temperature [32] and implementations of simple quantum error correction protocols [21].

The authors acknowledge P. Bertet, J. Wrachtrup, and M. Lecrivain for fruitful discussions and experimental assistance. This work was supported by the Agence Nationale de la Recherche (ANR) through the Projects DIAMAG, ADVICE and QINVC. J. R. M. acknowledges support from Conicyt Fondecyt, Grant No. 11100265, and U.S. Air Force Grant No. FA9550-12-1-0214.

*vjacques@lpqm.ens-cachan.fr

[1] N. A. Gershenfeld and I. L. Chuang, Science **275**, 350 (1997).
[2] B. E. Kane, Nature (London) **393**, 133 (1998).
[3] T. D. Ladd, F. Jelezko, R. Laflamme, Y. Nakamura, C. Monroe, and J. L. O'Brien, Nature (London) **464**, 45 (2010).
[4] R. Vincent, S. Klyatskaya, M. Ruben, W. Wernsdorfer, and F. Balestro, Nature (London) **488**, 357 (2012).
[5] D. R. McCamey, J. Van Tol, G. W. Morley, and C. Boehme, Science **330**, 1652 (2010).
[6] M. Steger, K. Saeedi, M. L. W. Thewalt, J. J. L. Morton, H. Riemann, N. V. Abrosimov, P. Becker, and H.-J. Pohl, Science **336**, 1280 (2012).
[7] M. V. G. Gurudev Dutt, L. Childress, L. Jiang, E. Togan, J. Maze, F. Jelezko, A. S. Zibrov, P. R. Hemmer, and M. D. Lukin, Science **316**, 1312 (2007).
[8] L. Robledo, L. Childress, H. Bernien, B. Hensen, P. F. A. Alkemade, and R. Hanson, Nature (London) **477**, 574 (2011).
[9] P. Neumann, J. Beck, M. Steiner, F. Rempp, H. Fedder, P. R. Hemmer, J. Wrachtrup, and F. Jelezko, Science **329**, 542 (2010).
[10] P. C. Maurer *et al.*, Science **336**, 1283 (2012).
[11] G. Balasubramanian *et al.*, Nat. Mater. **8**, 383 (2009).
[12] J. M. Taylor, P. Cappellaro, L. Childress, L. Jiang, D. Budker, P. R. Hemmer, A. Yacoby, R. Walsworth, and M. D. Lukin, Nat. Phys. **4**, 810 (2008).
[13] L. Childress, M. V. Gurudev Dutt, J. M. Taylor, A. S. Zibrov, F. Jelezko, J. Wrachtrup, P. R. Hemmer, and M. D. Lukin, Science **314**, 281 (2006).
[14] F. Jelezko, T. Gaebel, I. Popa, M. Domhan, A. Gruber, and J. Wrachtrup, Phys. Rev. Lett. **93**, 130501 (2004).
[15] T. van der Sar, Z. H. Wang, M. S. Blok, H. Bernien, T. H. Taminiau, D. M. Toyli, D. A. Lidar, D. D. Awschalom, R. Hanson, and V. V. Dobrovitski, Nature (London) **484**, 82 (2012).
[16] P. Neumann, N. Mizuochi, F. Rempp, P. Hemmer, H. Watanabe, S. Yamasaki, V. Jacques, T. Gaebel, F. Jelezko, and J. Wrachtrup, Science **320**, 1326 (2008).
[17] G. D. Fuchs, G. Burkard, P. V. Klimov, and D. D. Awschalom, Nat. Phys. **7**, 789 (2011).
[18] E. Togan *et al.*, Nature (London) **466**, 730 (2010).
[19] A. Sipahigil, M. L. Goldman, E. Togan, Y. Chu, M. Markham, D. J. Twitchen, A. S. Zibrov, A. Kubanek, and M. D. Lukin, Phys. Rev. Lett. **108**, 143601 (2012).
[20] H. Bernien, L. Childress, L. Robledo, M. Markham, D. Twitchen, and R. Hanson, Phys. Rev. Lett. **108**, 043604 (2012).
[21] M. A. Nielsen and I. L. Chuang, *Quantum Computation and Quantum Information* (Cambridge University Press, Cambridge, England, 2000).
[22] L. Jiang *et al.*, Science **326**, 267 (2009).
[23] See Supplemental Material at http://link.aps.org/supplemental/10.1103/PhysRevLett.110.060502 for further information on the experimental methods, single-shot readout of another ^{13}C nuclear spin, as well as the models that were used to fit the data of Figs. 2(c) and 3.
[24] A. Dréau, M. Lesik, L. Rondin, P. Spinicelli, O. Arcizet, J.-F. Roch, and V. Jacques, Phys. Rev. B **84**, 195204 (2011).
[25] V. Jacques, P. Neumann, J. Beck, M. Markham, D. Twitchen, J. Meijer, F. Kaiser, G. Balasubramanian, F. Jelezko, and J. Wrachtrup, Phys. Rev. Lett. **102**, 057403 (2009).
[26] A. Gali, Phys. Rev. B **80**, 241204 (2009).
[27] B. Smeltzer, L. Childress, and A. Gali, New J. Phys. **13**, 025021 (2011).
[28] A. Dréau, J. R. Maze, M. Lesik, J.-F. Roch, and V. Jacques, Phys. Rev. B **85**, 134107 (2012).
[29] T. M. Babinec, B. J. M. Haussmann, M. Khan, Y. Zhang, J. R. Maze, P. R. Hemmer, and M. Lončar, Nat. Nanotechnol. **5**, 195 (2010).
[30] G. D. Fuchs, V. V. Dobrovitski, R. Hanson, A. Batra, C. D. Weis, T. Schenkel, and D. D. Awschalom, Phys. Rev. Lett. **101**, 117601 (2008).
[31] We note that without optical illumination, both nuclear spin states are expected to have identical and much longer relaxation times.
[32] W. Pfaff, T. H. Taminiau, L. Robledo, H. Bernien, M. Markham, D. J. Twitchen, and R. Hanson, Nat. Phys. **9**, 29 (2013).